

**Exploring ultraviolet astronomical polarimetry:
Results from the Wisconsin Ultraviolet Photo-Polarimeter Experiment (WUPPE)**

K.H. Nordsieck, A.D. Code, and C.M. Anderson

Department of Astronomy, University of Wisconsin, 475 N. Charter St, Madison WI 53706-1390 USA
and

M.R. Meade, B. Babler, D. E. Michalski, R.H. Pfeifer, and T.E. Jones

Space Astronomy Lab, University of Wisconsin, 1150 University Ave, Madison WI 53706-1390 USA

ABSTRACT

In December 1990, the Wisconsin Ultraviolet Photo-Polarimeter Experiment ("WUPPE") on the Astro-1 shuttle Spacelab mission obtained approximately eight hours of pioneering ultraviolet spectropolarimetric observations on more than 20 galactic and extragalactic objects. WUPPE is a 0.5m Cassegrain telescope coupled to a Monk-Gilleson spectrometer with a magnesium fluoride polarizing beamsplitter preceded by magnesium fluoride halfwave retarders. Two spectra from 135 to 330 nm with orthogonal polarization are detected simultaneously by a pair of intensified photodiode arrays; the polarization at each wavelength is derived from the difference between the two spectra, modulated by changing the angle of the optical axis of the retarder. The total system quantum efficiency is approximately 4%, polarimetric efficiency 75%, polarimetric stability $\pm 0.04\%$, and the instrumental polarization (obtained in-flight from observations of unpolarized stars) was less than 0.1%. The first flight measured for the first time the ultraviolet polarization induced by interstellar dust, the UV intrinsic polarization of the rapidly rotating "Be" stars, and the large polarization in a "hidden" active galactic nucleus. A second flight of Astro is currently scheduled for 1994.

1. INTRODUCTION

The technique of astronomical polarimetry extracts information from electromagnetic radiation which is highly complementary to spectroscopy. Until now, however, it has been applied extensively only in the visible and radio spectral bands. For instance, until three years ago, the only extra-solar-system polarimetric observations in the ultraviolet were balloon measurements made in 1968 by Gehrels and collaborators¹ of two stars in two near-UV broad-band filters. At the University of Wisconsin Space Astronomy Laboratory we are engaged in a number of related "scouting missions" for polarimetry in the vacuum ultraviolet. The first of these is WUPPE, a medium resolution spectropolarimeter for the 135-330 nm region, where visible-wavelength spectropolarimetric techniques can be extended through the use of magnesium fluoride polarimetric optics. WUPPE is designed primarily for point-source, high signal-to-noise linear polarization investigations which complement or extend visible-wavelength polarimetric results: interstellar polarization as a probe of the properties of interstellar dust, and intrinsic stellar polarization, probing the geometry of stellar envelopes.

WUPPE was one of three ultraviolet telescopes included in the Astro-1 mission. The shuttle Columbia, carrying the Astro payload, was launched on December 2, 1990. The instruments sharing a common pointing system with WUPPE were the Hopkins Ultraviolet Telescope (HUT, a spectrometer observing the wavelengths 90-170 nm) and the Ultraviolet Imaging Telescope (UIT, which obtained 40 arcmin images in the wavelengths 120-300 nm). During the following nine days ultraviolet polarization data were obtained for a variety of astronomical sources. It is the purpose of this paper to present an overview of the instrument design, pre-mission and in-flight calibration, and data reduction techniques.

2. INSTRUMENT DESIGN

2.1 Telescope

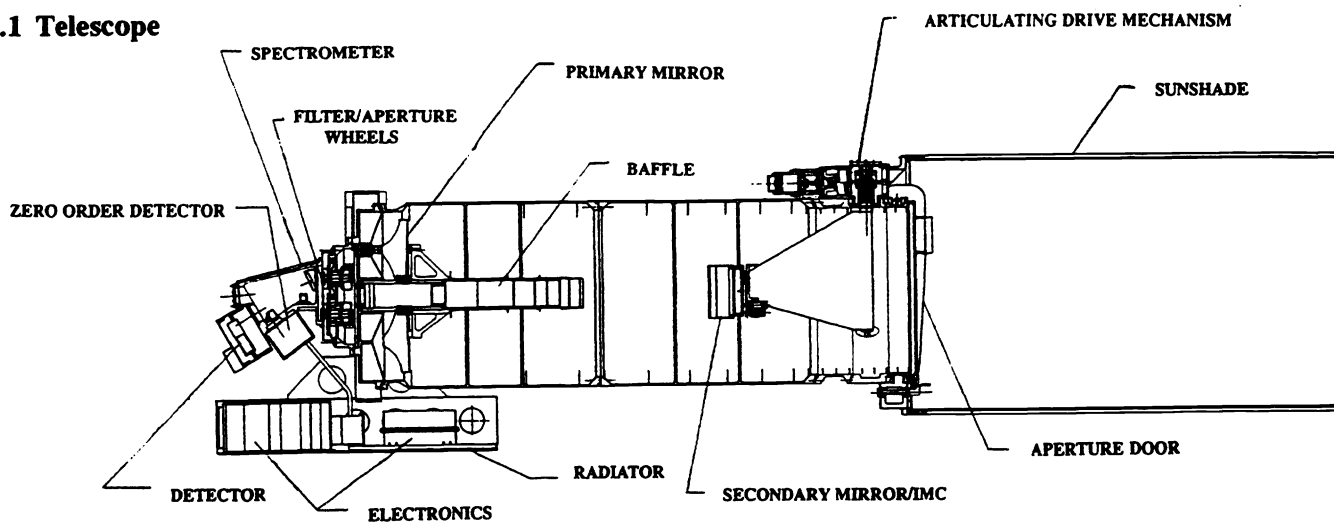


Figure 1. WUPPE Optical Overview

The WUPPE telescope is a 20-inch classical Cassegrain telescope. As light enters the telescope (from right, see Figure 1), it encounters an extensive sunshade fabricated by Heath-Tecna, Inc. from aluminum honeycomb with the inner honeycomb exposed and painted black. The sunshade allows for observations of stars brighter than magnitude 6 during the daytime part of the orbit. Next, a latchable aperture door provides for contamination protection during launch and re-entry (cleanliness is maintained on the ground with a dry N_2 gas purge). A Westinghouse deuterium hollow-cathode lamp mounted on a miniature optical bench in the door provides an ultraviolet continuum for checking system response on the ground. The telescope tube itself is fabricated from two rolled and welded aluminum tubes with internal baffles added. The primary mirror, an 0.5 m aperture $f/3$ parabola, consists of a light-weighted Schott Zerodur blank polished to $\lambda/4$, coated with a standard Al/MgF_2 coating. It is held by a three-point spider which penetrates the central hole of the mirror and which holds an extensive internal baffle. The hyperbolic secondary mirror completes an optical system with an effective $f/10$ focal ratio. For alignment, offsetting, and focussing, three secondary mirror vanes may be articulated independently. By pivoting the secondary mirror about the "neutral point" approximately 5 cm beyond the primary focal point, an offsetting capability of ± 15 arcmin is possible without appreciable image degradation (image diameter < 1.5 arcsec). In addition, the secondary mirror cell incorporates tip/tilt image motion compensation (IMC) through two piezo-electric transducers commanded by signals from the Spacelab pointing system. This IMC system together with the pointing performance of the Spacelab instrument pointing system (IPS) is specified to provide a pointing jitter of less than ± 0.2 arcseconds, as required for maintenance of optimum spectral purity.

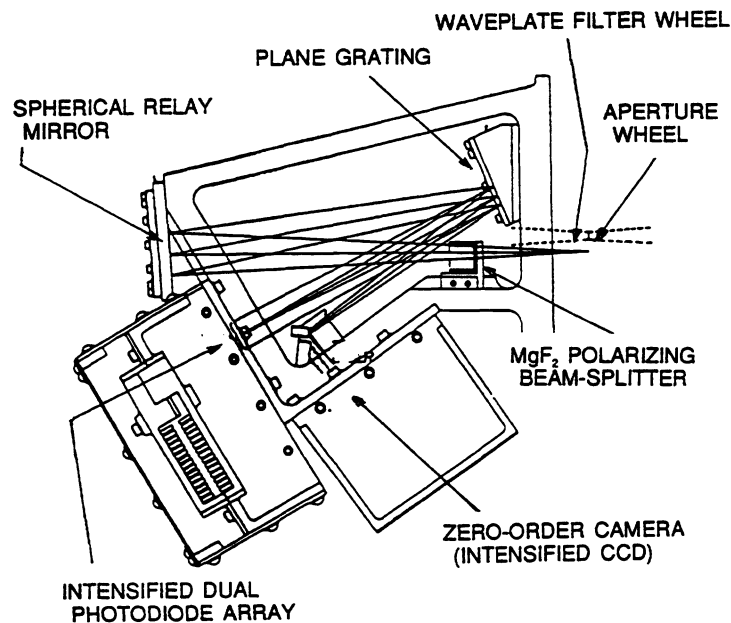


Figure 2. Spectropolarimeter Optical Diagram

2.2 Spectropolarimeter

The WUPPE spectropolarimeter (Figure 2) is a modified Monk-Gilleson spectrometer: a plane grating is placed between a spherical relay mirror and the detector. Again following the light path, at the focal plane of the telescope a 16-position aperture wheel serves to define the portion of the sky to be observed. The apertures (constructed of etched Corning Photoceram) include a 40 arcsec diameter acquisition aperture and a 4.2 arcsec diameter stellar aperture, in addition to a number of aperture shapes for diffuse sources, for instance 6x12 and 3x50 arcsecond rectangles. The 3 arcsec slit provides a spectral purity for a diffuse source of 0.6 nm. Next one encounters a polarimetric analyzer wheel which provides for modulation of the polarimetric state of the beam. A conventional linear polarization analyzer is provided by switching among a set of 3 pairs of matched $1/2\lambda$ MgF_2 retarders at angles of 0, 45, 15, 60, 30, and 75 degrees. An all-Stokes analyzer is provided by a MgF_2 Lyot plate which modulates the polarimetric state of the beam in wavelength, with different modulation patterns for the different Stokes parameters as described by Nordsieck². Next, a 1 cm MgF_2 Wollaston polarizing beam-splitter placed between the filter and the relay mirror splits the beam (perpendicular to the paper in Figure 2) into the two orthogonally-polarized beams. All the MgF_2 polarizing optics were fabricated by Karl Lambrecht Corp. After encountering a spherical relay mirror which provides a final $f/15$ beam, the light is dispersed by a 600 l/mm plane grating blazed at 190 nm, fabricated by Hyperfine, Inc. The grating is coated with Aluminum and overcoated with 500 Å MgF_2 .

At the spectrometer focal plane, the first order of the grating from 135 to 330 nm is seen as two orthogonally polarized 25mm long spectra, split by 3.5 mm. The image size parallel to the dispersion is less than 25 μ (0.2 nm in wavelength); the image size perpendicular to the dispersion is dominated by residual astigmatism: the angles of the relay mirror and grating in a standard Monk-Gilleson design are optimized to cancel astigmatism at the central wavelength; but the addition of the astigmatism from the Wollaston prism results in this point falling near the lowest wavelength for one split beam and near the highest wavelength for the other. The resulting astigmatic images are up to 0.5 mm in length.

Table 1. Estimated efficiency of WUPPE optical elements

Element	Effi	λ (nm)
Mirrors(3)	0.75	140 (min)
	0.90	200 (max)
Waveplate	0.91	Flat
Prism	0.50	140 (min)
	0.95	300 (max)
Grating	0.68	200 (max)
Detector	0.10	190 (max)
System	0.04	200 (max)

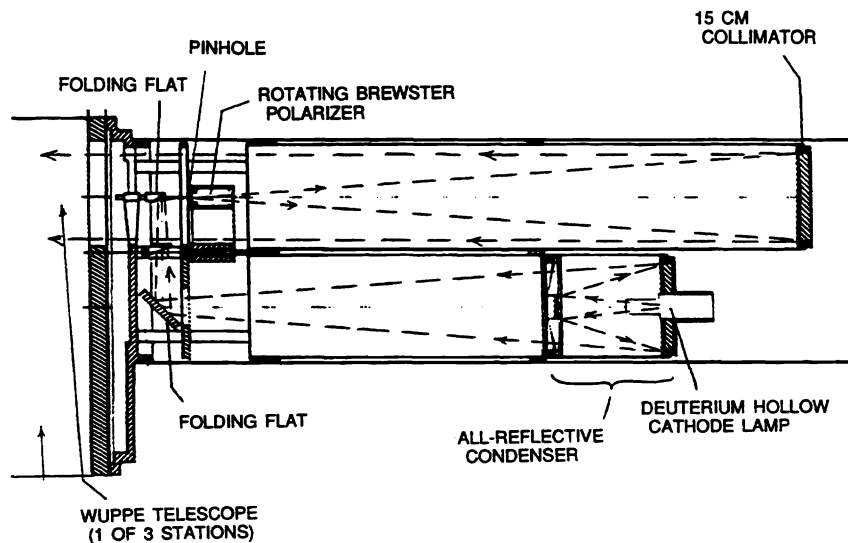


Figure 3. Ground Calibration Facility Optics

2.3 Detector

The detector is optimized for bright sources and large dynamic range. It consists of two parallel 1024-pixel Reticon photodiode arrays coupled to a single-stage ITT intensifier which converts the ultraviolet light to green phosphor light detectable by the photodiodes. In the intensifier, a Cesium Telluride photocathode on a MgF_2 window provides a solar-blind spectral coverage from 135-330 nm. A single straight channelplate is proximity-focused to the photocathode to provide an electron gain of 1000; these electrons are accelerated onto a P-1 phosphor (P-1, which does not have the persistent phosphorescent afterglow of the more frequently used

P-20, is more suitable for bright sources). The phosphor output of the intensifier is then fiberoptically coupled to the photodiode array. The diode pixels are $25\mu \times 2.5\text{ mm}$, and the arrays are separated by 3.5mm, thus matching the spectrometer format. The system peak quantum efficiency is 4% (see Table 1 for approximate efficiencies of each optical element). The combined maximum spectral resolution of the system is 0.6 nm. The detector is cooled to -35° C by a thermoelectric cooler and operated in analog integrating mode, with integration times from 0.2 sec to 128 sec, giving an input photon-limited dynamic range from 0 to 14^{th} magnitude stars. Because of the very high signal/noise required for polarimetry, most WUPPE targets were in the range 0-8 magnitude: readout integration times ("frames") were less than 8 seconds, so that a typical observation integration is the sum of many short frames. The zero order of the grating is relayed to an intensified CCD camera operating in the visible. This is used for acquisition and for monitoring of the pointing during an observation.

The instrument is controlled by a Motorola 6809 microprocessor, which commands Reticon and CCD readouts, mechanism motions, and science and housekeeping telemetry. An extensive library of observation sequences controls observations, while allowing for intervention by the Payload Specialist on board or by ground command. The output of the zero order camera is relayed to the shuttle aft flight deck video monitor for monitoring of the progress of the observation.

An instrument of similar design³, but with sensitivity to the visible wavelengths 320-760 nm was constructed for use on the University of Wisconsin Pine Bluff Observatory ("PBO") 36 inch telescope. This has been used in conjunction with WUPPE to develop science goals, verify the calibration by overlap at 320 nm, and to obtain time dependence information and simultaneous observations of targets observed by WUPPE.

3. CALIBRATION/PERFORMANCE

3.1 Ground calibration

Since there are no ultraviolet polarimetric standards in the sky, a detailed calibration of polarimetric efficiency was undertaken using a portable facility mounted on top of WUPPE at Kennedy Space Center (Figure 3 above): The light source is a Deuterium hollow-cathode lamp with an all-reflective condenser. After the condenser pinhole, a rotatable three-mirror (Al-MgF₂-Al) Brewster-angle polarizer provides 100% linearly polarized light from 150-330 nm. This illuminates a 15 cm collimator which can be rotated into one of three stations separated by

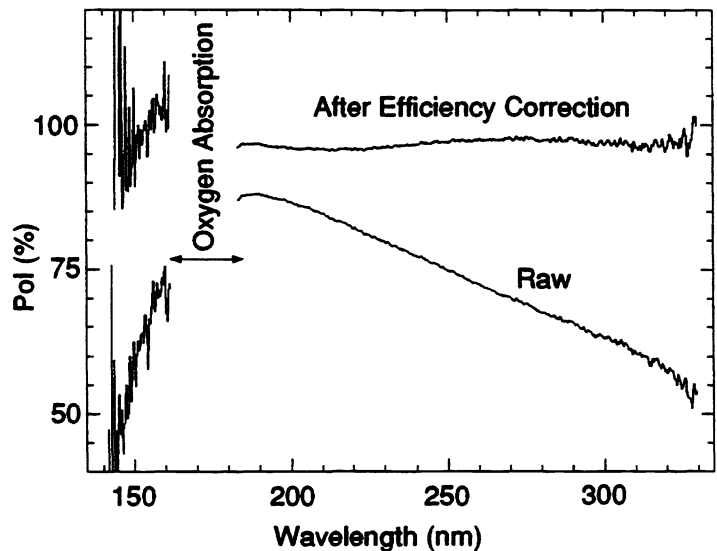


Figure 4. Halfwave Mode Polarimetric Efficiency

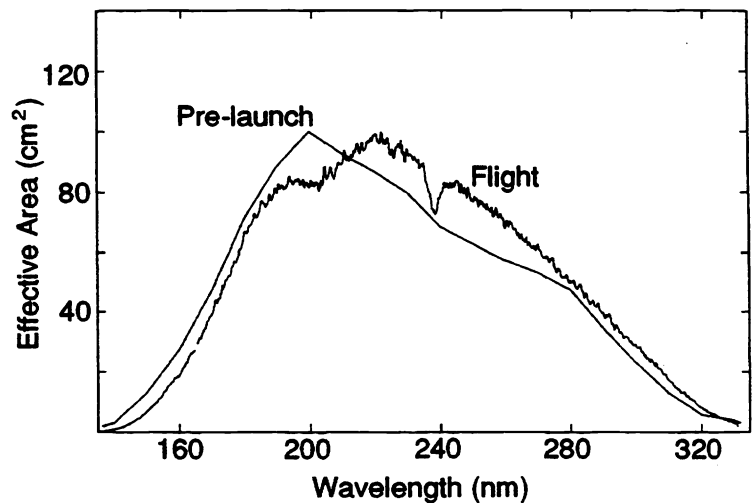


Figure 5. System effective area. Prelaunch estimate, flight calibration.

120° around the axis of the 50 cm WUPPE primary mirror. The calibration optics and WUPPE are then purged with argon gas, giving usable transmission to 150 nm. Data collected in this configuration were used to validate a model of the halfwave plates (see Appendix) and Lyot analyzers and to calibrate the internal scattered light. The scattered light was evaluated by examining the residual signal at the ends of the spectrum where the sensitivity drops to zero: it was modelled as a linear ramp from 0.1% of the mean signal at the blue end to 0.9% at the red end. Figure 4 illustrates the apparent polarimetric efficiency of the halfwave mode, before and after correction for waveplate retardation wavelength dependence, beam convergence effects and scattered light.

3.2 Flight Calibration

The wavelength dependence of the flux response curve was calibrated using stars of known ultraviolet flux from observations by the International Ultraviolet Explorer (IUE) and (for wavelengths greater than 320 nm) the Orbiting Astronomical Observatory (OAO). The relative flux calibration includes a correction for second-order contamination of the 280-330 nm spectrum by 140-165 nm light. The relative flux calibration is repeatable to approximately $\pm 10\%$. The absolute detector response was calibrated by evaluating the noise in the polarimetric signal for fainter targets, to give an effective quantum efficiency (since the detector is analog, photon counts are not available). The resulting absolute flux response curve is shown as a system effective area (summing the two orthogonal spectra) in Figure 5 above. The feature near 240 nm is due to a detector flaw appearing in the "A" polarimetric channel. The effective area curve agrees well with prelaunch predictions. Due to pointing system problems the absolute fluxes of some targets observed through smaller apertures are low by up to a factor of two.

The halfwave polarimetric efficiency calibration was checked using highly polarized stars observed nearly simultaneously in the visible at Pine Bluff Observatory (Figure 6). Since the polarization at 320 nm is very sensitive to the calibration, the agreement seen is very satisfactory. The polarimetric efficiency calibration is good to 1 part in 20. The Lyot mode calibration (in progress) will be done by cross-calibration using HD25443. The relative position angles of the analyzer filters was calibrated in the ground calibration (see Appendix). The absolute position angle was checked using the overlap region of highly polarized stars observed at PBO. The position angle calibration is repeatable to better than $\pm 1^\circ$.

The ultraviolet instrumental polarization was calibrated using stars known to be unpolarized in the visible. The primary standards were γ Gem and α Aur, with the red portion of α Hyi and the central portion of ψ Vel used as a check. The latter two stars were observed in an attempt to detect the onset of polarimetric effects

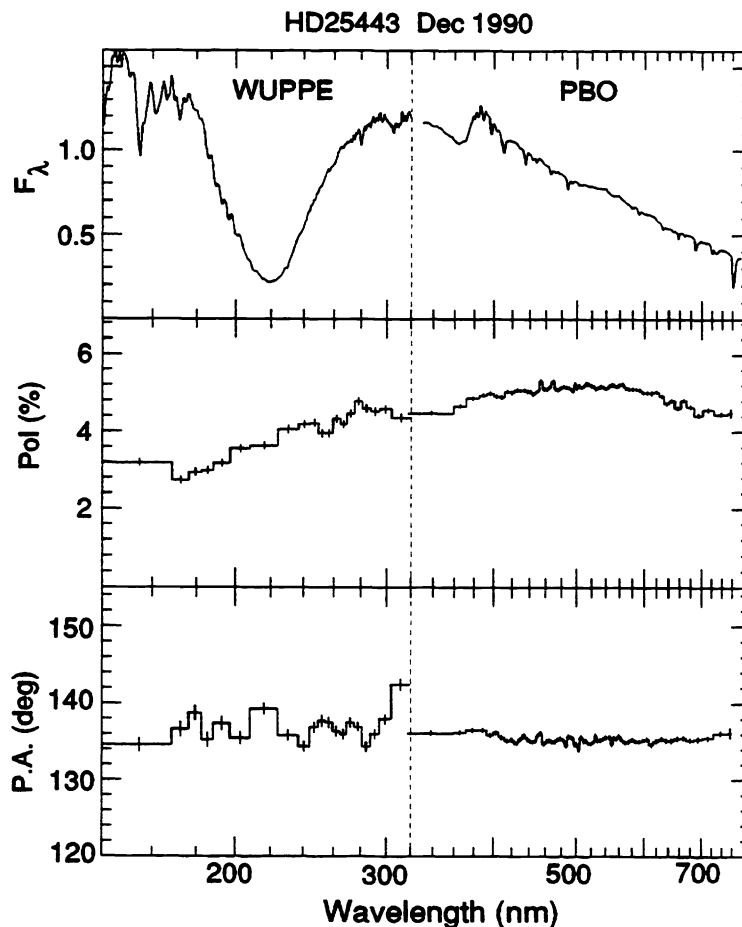


Figure 6. The polarized standard star HD 25443. Top: Flux ($\times 10^{-11}$ erg/s/cm²×Å). Middle: % linear polarization. Bottom: polarization position angle. Left: WUPPE, binned to 0.1% error; Right: PBO, binned to 0.05% error.

of rapid rotation, which had been predicted⁴ to appear only below 180 nm. All four stars have measured visible-wavelength polarization⁵ $< 0.01\% \pm 0.006\%$. Figure 7 shows the three highest signal/noise observations (two of γ Gem, one of α Hyi) along with the adapted instrumental polarization (smooth curve), averaging about 0.05%. The U Stokes parameter observations agree to about 0.05%, while the Q parameter shows about 0.1% system noise. The remaining system noise is thought to be due to the residual effects of pointing variations.

4. REDUCTION AND ANALYSIS

The flight data is reduced using a reduction and analysis program already in use with the visible-wavelength spectropolarimeter at the University of Wisconsin Pine Bluff Observatory. Steps include:

Several components of the background must be removed. First, cosmic ray events in the detector are seen as large spikes in single frames. Second, a timing problem in the telemetry electronics resulted in occasional single-pixel digital errors which were recognizable by their bit pattern and by comparison of redundant telemetry streams. Both are removed by replacement with the average of unaffected frames through the same analyzer filter. Third, thermal background in the photodiodes, which has a smooth dependence on pixel, was removed using background integrations obtained before and after the science observation, normalized to the signal at very low wavelengths where the response to light is negligible. Fourth, thermal photon events from the photocathode were evaluated from several long observations of background (eg, undetectable targets of the other instruments) during orbital night. Finally, background from the "sky" was dominated by solar scattered light in the daytime. This could be evaluated using three analog bright object sensors (phototransistors) mounted within the sunshade at the aperture door. Several observations obtained at solar angles less than 90° were contaminated in the longer wavelengths by this source. Orbital nighttime sky sources (zodiacal light, NO residual airglow) were not detected, as predicted prelaunch.

Removal of the residual effects of image motion proved to be problematic due to poor performance by the Spacelab Instrument Pointing System. For most of the mission, the IPS did not attain a closed-loop "optical hold" and the observations were hand-guided by the crew using video images of the star-field and a hand paddle. This resulted in image motion an order of magnitude greater than specification, which was in most cases beyond the operational capability of the IMC system. The result was a degradation in spectral purity and, most seriously, a time-dependent pixel response which compromised the precision of the polarimetry. However, some of these effects could be removed by a frame-by-frame pointing correction procedure: The target image in the zero-order camera and data from the image motion compensation system could be used to establish the image position for a given frame. Parallel to the dispersion, a simple shift restored some of the spectral purity; perpendicular to the dispersion, a table of pixel response variation was developed using the brightest stars, and was applied to each frame, so that each frame was referenced to the detector gain at a single standard point on the detector. These procedures resulted in an ultimate spectral purity of 2.5 nm and a signal/noise which approached input photon limited.

For halfwave mode data, three normalized "filter-pair differences" were formed pixel-by-pixel from the

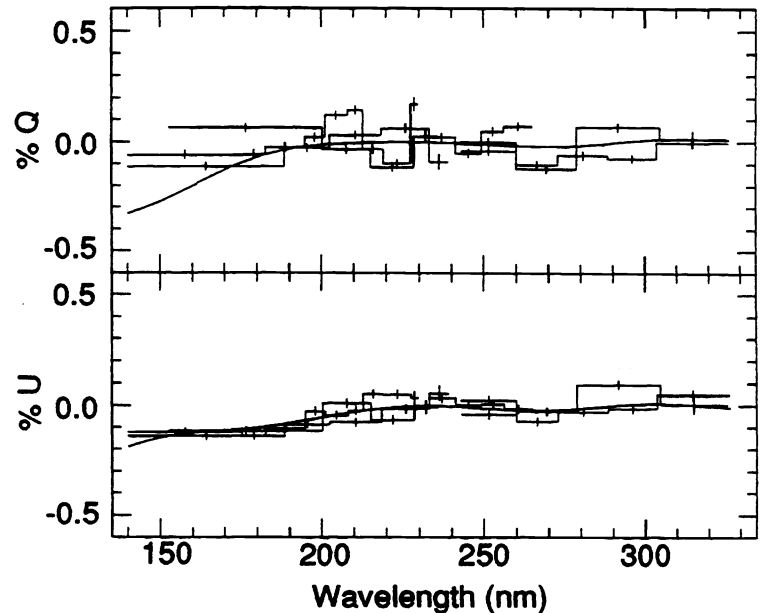


Figure 7. Instrumental linear polarization. Q, U stokes parameters (percent) for two observations of γ Gem and one of α Hyi, binned to constant error of 0.02%. Curve shows adopted instrument polarization.

response of the two split spectra "A" and "B" through two halfwave filters with optic axes 45° apart. These filter pairs correspond to orthogonal rotations of the input linear polarization. For instance, a difference spectrum $d(0)$ is formed from A and B spectra through the halfwave filters at angles 0° and 45° as follows:

$$d(0) = (A(0) - A(45))/(A(0) + A(45)) - (B(0) - B(45))/(B(0) + B(45))$$

and similarly for $d(15)$ and $d(30)$ using angle pairs (15°,60°) and (30°,75°). From the waveplate model one knows the (roughly sinusoidal) dependence of $d(\phi)$ on ϕ given input Stokes parameters $Q(\lambda)$ and $U(\lambda)$,

$$d(\phi) = d_Q(\lambda) Q/I + d_U(\lambda) U/I \quad (1)$$

A weighted linear least squares fit of the three $d(\phi)$ then yields $Q(\lambda)/I$, $U(\lambda)/I$, and $\epsilon(\lambda)$, where ϵ is an estimate of the mean error in Q/I and U/I . In practice, the data is divided into many independent sets, and the error-weighted mean of the independent data sets yields the final Q,U,ϵ spectrum. This formulation has been found to be insensitive to changes in total received flux due to pointing errors, gain changes in the detector, and noise events in the image tube.

The above polarimetric analysis does not depend on the absolute response of the system. In order to obtain an absolute flux spectrum, additional standard flux reduction techniques were applied to the sum of the two polarimetric channels A and B: The spectrum of a hot white dwarf (G191B2B) was used to derive a "flat-field" spectrum which gives the relative pixel-to-pixel response variations at the reference detector point. The raw flux spectra were divided by this flat-field and multiplied by a smooth flux response curve derived from ultraviolet flux standards.

Figure 6 above illustrates the standard data product of the reduction: a three-part spectrum showing the flux spectrum, linear polarization spectrum, and linear polarization position angle $\theta = 0.5 \tan^{-1} (U/Q)$. The polarization is usually "binned" (neighboring pixels averaged) until a constant mean error is achieved, to further improve the signal-to noise. Finally, a standard set of spectropolarimetric analysis tools (vector arithmetic, Q-U vector plots, wavelength dependence fitting) is used for scientific interpretation.

5. OBSERVATION SUMMARY

A summary of polarimetric observations obtained during Astro-1 is given in Table 2.

Table 2

Type	Name	Pol	Spc	Ref	Remark	Type	Name	Pol	Spc	Ref	Remark
Pol Standard	γ Gem	FG	G		Unpol	Chromospheric	α Aur	FG	G		Unpol
	HD 25443	G	G	6	Pol	Cataclysmic	UX UMa	L	F		
Solar System	Io	L	F			Plan Neb	NGC 1535	L	G		
Supergiant	κ Cas	G	G	7		Refl Neb	NGC 7023	L	P		
	α Cam	G	G	6	2 Obs	Interstellar Pol	HD 62542	FG	G	6	
	α Ori	G	G				HD 37903	G	G	6	
	HD 45677	G	G	8			HD 99264	G	G	6	
	P Cyg	F	G	7			HD 197770	G	G	6	2 Obs
Be	ζ Tau	G	G	9		Normal Galaxy	M31	L	P		
	p Car	F	G	10			M33	L	F		
	π Aqr	G	G	9	2 Obs		M74	L	P		
Wolf-Rayet	EZ CMa	G	G	11			M82	L	P		
	θ Mus	G	G	11		Active Galaxy	Mkn 335	L	G		
Rapid Rot.	α Hyi	FG	G		Red unpol		NGC 1068	G	G	12	2 Obs
	ψ Vel	F	G			QSO	3C273	L	G		
White Dwarf	Gr+70 8247	L	G				Q1821	L	G		

The overall quality (Poor, Fair, Good) of the polarimetry and spectroscopy is given, together with references for the initial reports on the listed objects. The Lyot mode analysis ("L") is in progress. In addition to these objects, approximately 20 faint targets chosen by the other experiments on the pointing system received sufficient exposure for adequate spectroscopy, but were of insufficient signal/noise for polarimetry.

6. ACKNOWLEDGEMENTS

WUPPE is supported by NASA contract NAS5-26777.

7. APPENDIX: HALFWAVE POLARIMETRIC EFFICIENCY MODEL

The limited choice of birefringent materials in the ultraviolet led to a fairly simple choice of polarimetric analyzer. The WUPPE halfwave filters are double-plate MgF₂ retarders obtained from Karl Lambrecht Corp. In this device, two 3-mm MgF₂ elements with retardation differing by 1/2λ at 190 nm are optically contacted with optic axes crossed. The retarder is used in an f/10 diverging beam. Two effects cause the response of the instrument to be reduced from a simple unit-amplitude sinusoidal dependence on axis angle, given an input 100% linear polarization. First, the birefringence wavelength dependence of MgF₂ leads to a variation of the phase retardation from 1/2λ at different wavelengths ("chromatic" effects). Second, the phase retardation at a particular wavelength varies with angle of incidence and with the angle between its plane of incidence and the optic axis. The combination of these two effects leads to a further reduction in efficiency, and a possible non-sinusoidal variation in polarimetric signal with retarder angle, which is modelled as follows:

Serkowski¹³ gives the phase retardation τ (in radians) of a single plate with thickness s, and ordinary and extraordinary indices of refraction n_o and n_e, for a ray making a small angle i with the normal in a plane with angle ω to the optic axis:

$$\tau \sim 2\pi(n_e - n_o)(s/\lambda)[1 - i^2/2n_o(\cos^2 \omega / n_o - \sin^2 \omega / n_e)] \quad (2)$$

For small birefringence Δn/n ≡ (n_e - n_o)/n, this is to first order,

$$\tau \sim 2\pi \Delta n (s/\lambda) [1 - i^2/2n_o^2 \cos^2 \omega] \quad (3)$$

For two crossed waveplates with thicknesses s₁ and s₂, the net retardation is then,

$$\begin{aligned} \tau_1 - \tau_2 &= \tau(0) [1 - i^2/2n_o^2 (s_1 + s_2)/(s_1 - s_2) \cos 2\omega] \\ &= \tau(0) [1 - \delta (i/i_{\max})^2 \cos 2\omega] \end{aligned} \quad (4)$$

where $\delta \equiv (i_{\max}^2/2n_o^2) (s_1 + s_2)/(s_1 - s_2)$

Here τ(0) is the normal retardation and δ is a measure of the maximum effect of beam convergence, which occurs at i = i_{max}. For instance, for WUPPE, with i_{max} = .05 rad, s₁ + s₂ = 6 mm, and s₁ - s₂ = 7.5 μm, δ = 0.52 (a quite large effect). Now the intensity after passing this beam through a polarizing beamsplitter (assuming 100% efficiency) is

$$I_{\pm} = 1/2 I [1 \pm q (1-H + H \cos 4\phi) \pm u H \sin 4\phi] \quad (5)$$

where "+" and "-" are the two orthogonally polarized beams, q = Q/I and u = U/I are the relative linear Stokes parameters of the incoming beam, φ is the angle between the waveplate optic axis and the positive Q direction, and H = 1/2 (1 - cos τ). In terms of the "difference spectra" defined in equation (1),

$$d(\phi) = q (1-H + H \cos 4\phi) + u H \sin 4\phi \quad (6)$$

For a perfect $1/2\lambda$ plate $H = 1$, and one has the usual sinusoidal response. To obtain the system efficiency in the general case one must average H (or $\cos \tau$) over all beam angles. Defining ψ to be the angle between the plane containing the ray and the normal and the positive Q direction, we have $\omega = \psi - \phi$, and thus the effective response for a waveplate at angle ϕ :

$$\langle \cos \tau \rangle(\phi) \equiv \int_i \int_\psi \cos \tau(i, \psi - \phi) i \, di \, d\psi / \int_i \int_\psi i \, di \, d\psi, \quad (7)$$

where the integral is taken over the beam illuminating the waveplate. If the beam is circularly symmetric, the zero-point of ψ is arbitrary, and $\langle \cos \tau \rangle$ is a constant independent of ϕ . This is effectively a demodulation which can be calculated (or removed by calibration). If the beam is asymmetric (i.e. with asymmetric vignetting) $\langle \cos \tau \rangle$ becomes dependent on ϕ so that $d(\phi)$ is no longer sinusoidal. For a first-order ($\cos 2\phi$) beam asymmetry, we find,

$$\langle \cos \tau \rangle \sim D_0 \cos [\tau(0) + D_1 \cos 2\phi], \quad (8)$$

where $D_0 = \langle \cos [\tau(0) \delta (i/i_{\max})^2 \cos 2\phi] \rangle$
and $D_1 = \langle \sin [\tau(0) \delta (i/i_{\max})^2 \cos 2\phi] \rangle$.

D_0 is an additional demodulation present in all finite beams; D_1 is non-zero only for asymmetric beams, and results in a non-sinusoidal $d(\phi)$ dependence.

The birefringence of MgF_2 was represented (cf data in Chandrasekharan and Damany¹⁴) by the following fit, valid from 135 -330 nm:

$$\Delta n(\lambda) = 0.0115 [1 + 0.0075/\lambda^2 - (0.0085/(\lambda-0.118))^2], \quad (9)$$

where λ is in μm . The instrumental parameters for the WUPPE system were finally obtained from the ground calibration data, which consisted of complete observations (six filter angles) of 100% linearly polarized light at 7 angles (0-90 in 15° steps). The three off-axis illumination stations were summed to give a nominally symmetric beam. A nonlinear least squares fit of the resulting $7 \times 3 = 21$ $d(\phi)$ spectra to the above model yielded values for the angles of the six waveplates, for the wavelength at which the plates are $1/2$ wave (190 nm), and for D_0 and D_1 . D_0 and D_1 were within errors of the theoretical values for the calibration facility beam (0.81 and 0, respectively), verifying the model. The theoretical values for the fully-illuminated WUPPE beam were then adopted, $D_0 = 0.773$ and $D_1 = 0$.

7. REFERENCES

1. T. Gehrels, "Wavelength dependence of polarization. XXVII. Interstellar polarization from 0.22 to 2.2 μm ," *Astronomical Journal* **79**, pp. 591-593, 1974.
2. K.H. Nordsieck, "A simple polarimetric system for the Lick Observatory image-tube scanner," *Pub. Astronomical Society of the Pacific* **86**, pp. 324-329, 1974.
3. K.H. Nordsieck, B. Babler, K.S. Bjorkman, M.R. Meade, R.E. Schulte-Ladbeck, and M.J. Taylor, "Stellar spectropolarimetric monitoring at the University of Wisconsin," Nonisotropic and Variable Outflows from Stars, ed. Drissen, Leitherer, and Nota, pp. 114-117, Astronomical Society of the Pacific, San Francisco, 1992.
4. C.M. Anderson and L.R. Doherty, "Ultraviolet polarimetry of rotating A and F stars," (Abstract) *Bull. American Astronomical Society* **22**, pp. 867-868, 1990.

5. J. Tinbergen, "Interstellar polarization in the immediate solar neighborhood," *Astronomy and Astrophysics* **105**, pp. 53-64, 1982.
6. G.C. Clayton, C.M. Anderson, A.M. Magalhães, A.D. Code, K.H. Nordsieck, M.R. Meade, M.J. Wolff, B. Babler, K.S. Bjorkman, R.E. Schulte-Ladbeck, M.J. Taylor, and B.A. Whitney, "The first spectropolarimetric study of the wavelength dependence of interstellar polarization in the ultraviolet," *Astrophysical Journal*, **385**, pp. L53-L57, 1992.
7. M. Taylor, A.D. Code, K.H. Nordsieck, C.M. Anderson, B.L. Babler, K.S. Bjorkman, G.C. Clayton, A.M. Magalhães, M.R. Meade, R.E. Schulte-Ladbeck, and B.A. Whitney, "First ultraviolet spectropolarimetry of hot supergiants," *Astrophysical Journal* **382**, pp. L85-L88, 1991.
8. R.E. Schulte-Ladbeck, D.S. Shepherd, K.H. Nordsieck, A.D. Code, C.M. Anderson, B.L. Babler, K.S. Bjorkman, G.C. Clayton, A.M. Magalhães, M.R. Meade, M. Taylor, and B.A. Whitney, "Evidence for a bipolar nebula around the peculiar B[e] star HD 45677 from ultraviolet spectropolarimetry," *Astrophysical Journal* **401**, pp. L105-L108, 1992.
9. K.S. Bjorkman, K.H. Nordsieck, A.D. Code, C.M. Anderson, B.L. Babler, G.C. Clayton, A.M. Magalhães, M.R. Meade, M.A. Nook, R.E. Schulte-Ladbeck, M. Taylor, and B.A. Whitney, "First spectropolarimetry of Be stars from the Wisconsin Ultraviolet Photo-Polarimeter Experiment," *Astrophysical Journal* **383**, pp. L67-L70, 1991.
10. K.S. Bjorkman, M.R. Meade, K.H. Nordsieck, C.M. Anderson, B.L. Babler, G.C. Clayton, A.D. Code, A.M. Magalhães, R.E. Schulte-Ladbeck, M. Taylor, and B.A. Whitney, "Ultraviolet spectropolarimetry of the Be star PP Carinae with WUPPE," *Astrophysical Journal* in press, Aug 1, 1993.
11. R.E. Schulte-Ladbeck, K.H. Nordsieck, A.D. Code, C.M. Anderson, B.L. Babler, K.S. Bjorkman, G.C. Clayton, A.M. Magalhães, M.R. Meade, D. Shepherd, M. Taylor, and B.A. Whitney, "The first linear polarization spectra of Wolf-Rayet stars in the ultraviolet: EZ Canis Majoris and θ Muscae," *Astrophysical Journal* **391**, pp. L37-L40, 1992.
12. A.D. Code, M.R. Meade, C.M. Anderson, K.H. Nordsieck, G.C. Clayton, B.A. Whitney, A.M. Magalhães, B. Babler, K.S. Bjorkman, R.E. Schulte-Ladbeck, and M.J. Taylor, "The first ultraviolet spectropolarimetric study of NGC 1068," *Astrophysical Journal* **403**, pp. L63-L65, 1993.
13. K. Serkowski, "Polarimeters for optical astronomy," Planets, Stars, and Nebulae studied with photopolarimetry, ed. T. Gehrels, pp. 135-174, The University of Arizona Press, Tucson, Arizona, 1974.
14. V. Chandrasekharan and H. Damany, "Anomalous dispersion of birefringence of sapphire and magnesium fluoride in the vacuum ultraviolet," *Applied Optics* **8**, pp. 671-675, 1969.